



Mohammad Hossein SANGDANI <sup>1</sup>, Alireza TAVAKOLPOUR-SALEH <sup>1</sup>

## Predicting performance and onset criteria of a three-stage double-acting thermoacoustic Stirling oscillator: Analysis and experiment

Received 27 January 2024, Revised 13 October 2024, Accepted 21 October 2024, Published online 28 November 2024

**Keywords:** thermoacoustic oscillator, regulator system, onset criteria, three-stage, double acting

In this paper, a novel analytical approach is proposed to predict the performance and onset criteria of a three-stage double-acting thermoacoustic Stirling oscillator (TDTASO). First, a coupled dynamic-thermodynamic model justifying the behavior of TDTASO is presented, taking into account Schmidt's theory assumptions. Subsequently, the manipulation of the obtained governing equations reveals that the considered Stirling oscillator is a physical regulator system. Thus, the onset criteria, which are the necessary conditions for designing such oscillators, are assessed based on a new analytical method resulting from a regulator-like model. Accordingly, the onset temperature difference is predicted corresponding to different dimensions of the resonator section in the TDTASO. Next, the sensitivity of the TDTASO to the inconsistency of resonators' dimensions is investigated. The results show that increasing the length of the mismatched water column results in a higher frequency. Finally, a prototype TDTASO is constructed and experimentally evaluated. Accordingly, the oscillator frequency is measured 3.14 Hz corresponding to the onset temperature of 163°C and the resonator length of 0.52 m. The experimental data demonstrate the effectiveness of the proposed analytical scheme in predicting the necessary conditions for designing the TDTASO.

### 1. Introduction

The growing request of world countries to new resources of clean energy and the challenges pertaining to the fossil fuels consumptions have led researchers to the renewable energies. The Stirling engines are among the most popular renewable

---

✉ Alireza TAVAKOLPOUR-SALEH, e-mails: [tavakolpouralireza@gmail.com](mailto:tavakolpouralireza@gmail.com), [tavakolpour@sutech.ac.ir](mailto:tavakolpour@sutech.ac.ir)

<sup>1</sup>Department of Mechanical Engineering, Shiraz University of Technology, Shiraz, Iran



© 2024, The Author(s). This is an open-access article distributed under the terms of the Creative Commons Attribution (CC-BY 4.0, <https://creativecommons.org/licenses/by/4.0/>), which permits use, distribution, and reproduction in any medium, provided that the author and source are cited.

energy converters that can be used to convert renewable energies such as solar radiation or biogases into mechanical work and then, electricity.

The first type of Stirling engines, known as kinematic Stirling engines (KSEs), was introduced by Robert Stirling in 1816 and is currently available with alpha, beta, and gamma configurations [1]. These engines are characterized by their solid pistons, crankshaft, and flywheel, which are connected together with rigid links. However, KSEs face challenges such as mechanical friction, sealing problems, and relatively high construction and maintenance costs [1]. To address these issues, researchers have attempted to modify and optimize the design of these kinematic engines, leading to the development of a new advanced type of Stirling engines called dynamic Stirling engines (DSEs) [2, 3]. DSOs include free piston engines [4], Fluidyne engines, and thermoacoustic engines [5]. The free piston Stirling Engines (FPSEs), first presented by Weale [1], addressed some drawbacks of KSEs but still faced issues with mechanical friction. To tackle the sealing problem, researchers proposed Fluidyne Stirling engines [1, 6], which utilized liquid pistons to resolve sealing issues but faced reduced operating frequency due to the high weight of the liquid pistons, limiting efficiency [7]. Subsequently, to overcome the challenges of free piston and Fluidyne engines, a new type of Stirling engine, the thermoacoustic Stirling engines (TASEs), was developed. The first design of a TASE was presented by Backhaus and Swift in 1999 [7, 8]. TASEs addressed many problems associated with previous engines [9, 10] and can be considered a modern version of FPSEs. In 2005, Luo et al. [11] developed a traveling-wave thermoacoustic heat engine that comprised a resonance tube in a tapered shape. The tapered resonance tube was used to prevent the incidence of shock waves and energy shift at dominant frequency. In fact, the proposed engine by Luo et al. operated based on a combination of traveling and standing acoustic waves, in such a way that the acoustic field was a traveling-wave in the looped tube and a standing-wave in the resonance tube. Despite the unique benefits of the presented engine, there were two drawbacks concerning this engine, as well. First, the long length of the resonance tube severely limited the application of this engine. Second, achieving a perfect energy accumulation in the resonance tube was impossible that reduced the efficiency of this engine. Zhang et al. [12] proposed a double-acting traveling-wave thermoacoustic Stirling engine equipped with water column resonator which had a more compact configuration than the original TASEs. This engine contained three symmetrical series sections each of which included a core section and a resonance U-shape tube filled by water as the fluid piston. Due to the high density and inertia of water in the resonator section, this engine resolved the problem of long resonators in the previous model. Next, a double-acting gas-liquid traveling-wave thermoacoustic heat engine was studied numerically and experimentally in 2013 [13]. The simulation study was implemented via the DeltaEC software developed at the US Los Alamos Laboratory [14]. The proposed engine was tested under loaded and no-load conditions. Zhang and Luo [15] presented a double-acting traveling-wave thermoacoustic engine with water pistons. Their results showed that the maximal thermal efficiency

of the proposed engine was about 51% at 1500 K of the heat source temperature. This outcome revealed that the engine was so efficient. The influence of different operating gasses on the efficiency of a traveling-wave liquid-piston thermoacoustic Stirling engine was addressed by Li et al. [16]. They perused the resonant frequency, pressure ratio, and onset temperature of the engine under different mean pressures using nitrogen, helium, and carbon dioxide as working gases. They concluded that engine efficiency was strongly influenced by the type of operating gas. A numerical and experimental research work on the relationship between the number of series units and the performance of a doubleacting Stirling engines with liquid-pistons was conducted by Tamura et al. [17]. The obtained results demonstrated that the number of 3, 4 and 5 units were appropriate to achieve acceptable outcomes. Hyodo et al. [18] used a mass-spring model to analyze a liquid-piston traveling-wave engine. Then, by analyzing the hydrodynamic equation of the engine, they proved that the thermodynamic cycle of the operating gas resembled the Stirling cycle. The gas-liquid interface instability is one of the main problems concerning this liquid piston engines that is known as finite-amplitude oscillations. The reported results confirmed that the increase of gas pressure amplitude was usually limited by the unstable motion of liquid pistons. Murti et al. [19] proposed two methods to overcome these problems. The first technique was to use submerged polyethylene floats and the second was to increase the cross-section area of the tub. These methods effectively increased the pressure amplitude and decrease the instability motion of the liquid surface.

So far, many researchers employed momentum, continuity, and energy equations [20, 21] to investigate performance as well as to predict the onset criteria of TASEs. The analysis has been usually done through DeltaEC program [13, 15, 22]. In fact, this program uses linear thermoacoustic theory to simulate the thermoacoustic heat engines. Recently, a few mechanical models have been proposed for the analysis of thermoacoustic Stirling engines, some of which have been focused on the analogy between electrical and acoustical systems. These models have received more attention because they simplify the engine design process.

A review of the past research papers reveals the TDTASOs have not been considered as physical regulator systems and the overall performance and the corresponding onset criteria are predicted accordingly. Indeed, predicting the onset criteria of TDTASO is a critical issue to assure instability and triggering of the oscillator system at startup state which is the necessary condition to design of such complex thermally-driven oscillators. In this work, the similarity of the TDTASO dynamics to a regulator system is first revealed. Then, a new analytical model is proposed to justify the dynamic characteristics of the thermoacoustic oscillator as well as to predict the onset criteria. In comparison with the results of some papers presented previously in literature in which some researchers mistakenly stated the overall operating frequency of the oscillator is identical to the resonance frequency of the water columns, the crucial analysis and experimental data of this work show this has not been a valid finding. Besides, in this paper, the effect of mismatched

dimensions of each unit of the multi-stage oscillator on the overall performance and onset criteria of the oscillator is investigated. Finally, different numerical investigations are provided to show the effectiveness of the proposed design technique. Moreover, an experimental three-phase double-acting thermoacoustic Stirling oscillator equipped with water column resonators is manufactured and tested to verify the results predicted by the proposed analytical model.

## 2. Three-phase double-acting thermoacoustic Stirling oscillator with water column resonator

As depicted in Fig. 1, the TDTASO with water pistons system has three symmetrical stages, whilst each stage is composed of a regenerator, a hot heat exchanger, two cold heat exchangers (main and secondary), a thermal buffer tube, a U-shaped resonator and two joint tubes. The U-tubes filled with water act as pistons (i.e., resonators) in the TDTASO system. It is interesting to note that the motions of the two adjacent water columns in the considered thermoacoustic oscillator resemble the motions of solid pistons in a double acting free piston Stirling oscillator that works according to the Stirling cycle [23]. Fig. 2 shows PV diagram of the ideal Stirling cycle in which four thermodynamic states can be distinguished. These states are schematically represented by two solid pistons in Fig. 3. This figure shows that the cycle consists of two constant volume and two isothermal processes.

Process 1–2: Heat transfer is done to the operating gas (at temperature  $T_h$ ) and the operating gas is expanded in an isothermal process.

Process 2–3: Heat transfer is done from the operating gas to the regenerator in a constant volume process and the operating gas temperature reaches the cold space temperature  $T_c$ .

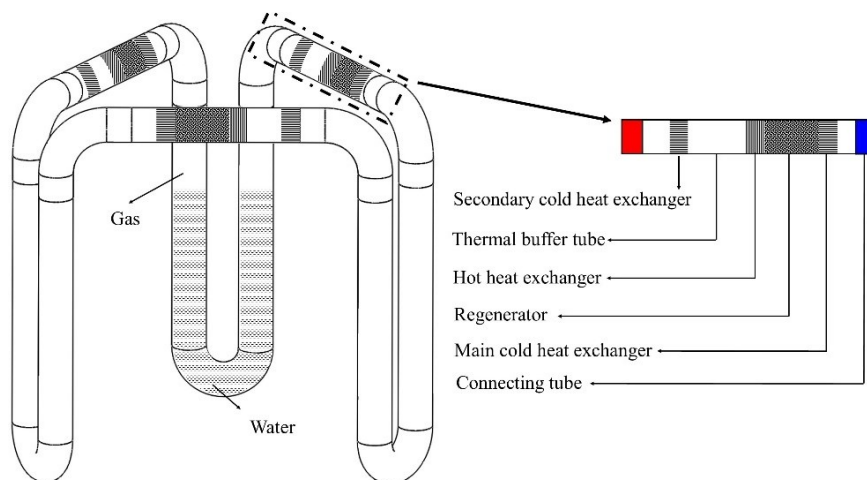


Fig. 1. Schematic of the TDTASO with water pistons

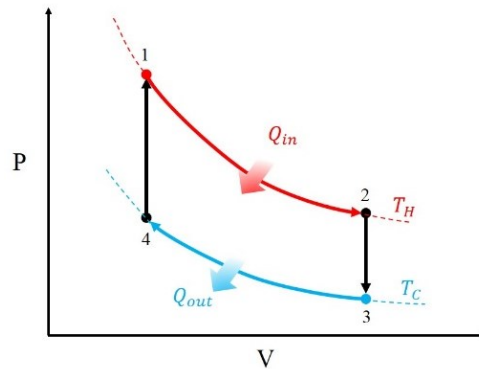


Fig. 2. Ideal Stirling cycle

Process 3–4: Heat transfer is done from the operating gas to the heat sink (at temperature  $T_c$ ) and the operating gas is compressed in an isothermal process.

Process 4-1: Heat transfer is done to the operating gas from regenerator in a constant volume process and the operating gas temperature reaches the hot space temperature  $T_h$ .

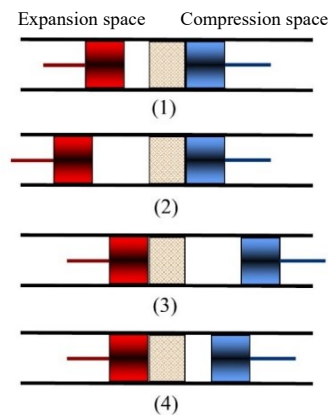


Fig. 3. Schematic representation of the four thermodynamic states in the ideal Stirling cycle resulting from the two opposed pistons

Indeed, the configuration of an alpha type Stirling oscillator has been depicted in Fig. 3 which can be taken into account as one unit of the considered TDTASO. It is clear that the standard alpha-type Stirling oscillator contains one cylinder and two pistons (i.e., compression and expansion pistons); whereas, in a three-phase double acting Stirling oscillator (see Fig. 1) there exists just one piston corresponding to each cylinder which has both compressing and expanding duties at the same time. The gradient of temperature between both ends of regenerator is an important factor providing required condition for generating acoustic power.

The required temperature gradient is made by the hot heat exchanger and the main cold heat exchanger installed at both ends of the regenerator section. This system is self-excited and the oscillation starts when the temperature discrepancy along the regenerator section exceeds a distinguished value (i.e., onset temperature difference). It is worth noting that one of the advantages of this type of TASEs is energy recovery from one unit to the next one because of its looped configuration, which results in a high efficiency. The phase difference between the motions of two adjacent water columns in a three-stage oscillator is 120 degrees inherently.

### 3. Mathematical background

As said before, if a lumped mechanical model is found for the thermoacoustic system, then, the TASEs can also be designed and analyzed based on the free piston Stirling oscillators viewpoint. Accordingly, in this study, an appropriate mechanical model of the TDTASO with water pistons is first acquired based on the similarities of the considered oscillator to the FPSEs. In this section, the dynamic equation of a single U-tube is first presented and then, the overall dynamics of the TDTASO with water column resonators is achieved based on the U-tube dynamics incorporating the Schmidt's theory.

#### 3.1. U-tube dynamics

Fig. 4 shows a U-tube filled with a liquid. A pressure difference is exerted at both ends of the U-tube that causes a level difference of  $2h$ . The dynamic equation is obtained according to the Newton's second law of motion applied to the column mass  $m$  of the liquid:

$$\sum F = ma, \quad (1)$$

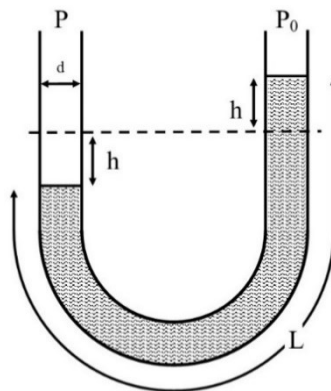


Fig. 4. A U-tube with pressure difference at both ends

where  $m$  (the mass of liquid) and  $a$  (acceleration) can be represented as:

$$m = \rho AL, \quad (2)$$

$$a = \ddot{h}. \quad (3)$$

Substituting Eqs. (2) and (3) into Eq. (1), yields

$$\sum F = \rho AL \ddot{h}, \quad (4)$$

where  $\sum F$  is the resultant of forces affecting the water column in the U-shape tube. The forces are given as:

$$\sum F = F_p + F_g + F_{\text{viscous}}, \quad (5)$$

where  $F_p$  is the force resulting from the pressure difference,  $F_g$  is the weight of the unbalanced section of liquid column and  $F_{\text{viscous}}$  is the damping force due to the viscosity of the liquid [24].

$$F_p = A(P - P_0), \quad (6)$$

$$F_g = 2\rho Agh, \quad (7)$$

$$F_{\text{viscous}} = \frac{32\mu AL}{d^2} \dot{h}, \quad (8)$$

where  $A$  is the cross sectional area of the tube,  $\rho$  is the density of the liquid and  $\mu$  is viscosity of the liquid. Substituting Eqs. (6)–(8) into Eq. (5) and using Eq. (4) the dynamic equation governing the U-tube resonator is obtained as:

$$\ddot{h} + \frac{32\mu}{\rho d^2} \dot{h} + \frac{2g}{L} h = \frac{1}{\rho L} (P - P_0). \quad (9)$$

### 3.2. Oscillator dynamics

In this research, the governing equations of the TDTASO system are given based on the Schmidt's theory. Accordingly, for deriving the mechanical model of the TDTASO this assumption is considered [3, 25]:

1. Instantaneous pressure is presumed to be equal at both sides of the regenerator in each oscillator's stage.
2. The gas temperature is constant within compression and expansion spaces.
3. The mass of the gas does not change in the thermodynamic cycle.
4. The operating gas is considered ideal.
5. The regeneration process is perfect.

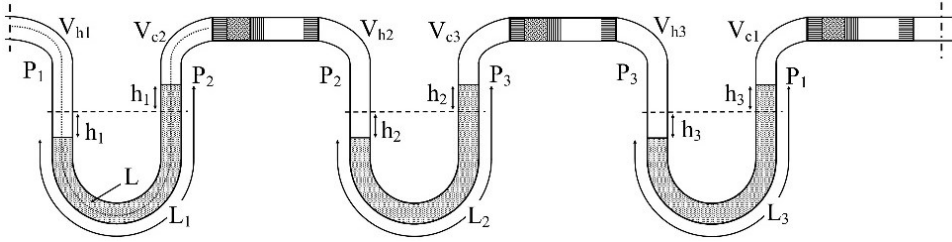


Fig. 5. Parameterized expanded schematic of the TDTASO

As demonstrated in Fig. 5 and based on the Schmidt's theory, the pressures at both ends of regenerators in each stage of the oscillator are equal. According to these assumptions and using Eq. (9), the dynamic equations governing the TDTASO with water column resonators can be expressed as follows:

$$\ddot{h}_1 + \frac{32\mu}{\rho d^2} \dot{h}_1 + \frac{2g}{L_1} h_1 = \frac{1}{\rho L_1} (P_1 - P_2), \quad (10)$$

$$\ddot{h}_2 + \frac{32\mu}{\rho d^2} \dot{h}_2 + \frac{2g}{L_2} h_2 = \frac{1}{\rho L_2} (P_2 - P_3), \quad (11)$$

$$\ddot{h}_3 + \frac{32\mu}{\rho d^2} \dot{h}_3 + \frac{2g}{L_3} h_3 = \frac{1}{\rho L_3} (P_3 - P_1). \quad (12)$$

The instantaneous pressure of the operating gas in the oscillator can be acquired using the Schmidt's theory and ideal gas law ( $PV = mRT$ ).

$$\hat{P}_1 = m_1 \left( \frac{V_{h1}}{RT_h} + \frac{V_{c1}}{RT_c} \right)^{-1}, \quad (13)$$

$$\hat{P}_2 = m_2 \left( \frac{V_{h2}}{RT_h} + \frac{V_{c2}}{RT_c} \right)^{-1}, \quad (14)$$

$$\hat{P}_3 = m_3 \left( \frac{V_{h3}}{RT_h} + \frac{V_{c3}}{RT_c} \right)^{-1}. \quad (15)$$

The volumes of expansion and compression spaces (i.e.,  $V_{h1}$ ,  $V_{h2}$ ,  $V_{h3}$ ,  $V_{c1}$ ,  $V_{c2}$ , and  $V_{c3}$ ) are functions of variables  $h_1$ ,  $h_2$  and  $h_3$  that make Eqs. (13)–(15) nonlinear. According to Fig. 5, these volumes are stated as:

$$V_{c1} = V_{c10} - Ah_3, \quad (16)$$

$$V_{h1} = V_{h10} + Ah_1, \quad (17)$$

$$V_{c2} = V_{c20} - Ah_1, \quad (18)$$

$$V_{h2} = V_{h20} + Ah_2, \quad (19)$$

$$V_{c3} = V_{c30} - Ah_2, \quad (20)$$

$$V_{h3} = V_{h30} + Ah_3. \quad (21)$$



Since a control-based design approach will be introduced in the next section, the governing equation must be declared in the state-space. Consequently, linearization of the pressure equations is essential in this place. Besides, at startup instant the oscillation amplitude of liquid column is small and linearization is reasonable. Hence, the nonlinear pressures are presented in Eqs. (13)–(15) are linearized around their initial volumes (i.e.,  $V_{c10}$ ,  $V_{h10}$ ,  $V_{c20}$ ,  $V_{h20}$ ,  $V_{c30}$ ,  $V_{h30}$ ) which are their equilibrium state. The linearization is done by the Taylor series as follows:

$$P \approx P_0 + \left. \frac{\partial \hat{P}}{\partial V_h} \right|_{V_h=V_{h0}}^{V_c=V_{c0}} (V_h - V_{h0}) + \left. \frac{\partial \hat{P}}{\partial V_c} \right|_{V_h=V_{h0}}^{V_c=V_{c0}} (V_c - V_{c0}). \quad (22)$$

Hence, the linearization of Eqs. (13)–(15) based on Eq. (22) results in the following linear pressure equations:

$$P_1 = P_0 - \frac{m_1 RA}{T_h B_1^2} h_1 + \frac{m_1 RA}{T_c B_1^2} h_3, \quad (23)$$

$$P_2 = P_0 - \frac{m_2 RA}{T_h B_2^2} h_2 + \frac{m_2 RA}{T_c B_2^2} h_1, \quad (24)$$

$$P_3 = P_0 - \frac{m_3 RA}{T_h B_3^2} h_3 + \frac{m_3 RA}{T_c B_3^2} h_2, \quad (25)$$

where,

$$B_1 = \frac{V_{h10}}{T_h} + \frac{V_{c10}}{T_c}, \quad (26)$$

$$B_2 = \frac{V_{h20}}{T_h} + \frac{V_{c20}}{T_c}, \quad (27)$$

$$B_3 = \frac{V_{h30}}{T_h} + \frac{V_{c30}}{T_c}. \quad (28)$$

At last, the TDTASO system dynamic equations are obtained by substituting Eqs. (23)–(25) into Eqs. (10)–(12) as follows:

$$\ddot{h}_1 + \frac{32\mu}{\rho d^2} \dot{h}_1 + \left( \frac{2g}{L_1} + \frac{m_1 RA}{\rho L_1 T_h B_1^2} + \frac{m_2 RA}{\rho L_1 T_c B_2^2} \right) h_1 - \frac{m_2 RA}{\rho L_1 T_h B_2^2} h_2 - \frac{m_1 RA}{\rho L_1 T_c B_1^2} h_3 = 0, \quad (29)$$

$$\ddot{h}_2 + \frac{32\mu}{\rho d^2} \dot{h}_2 + \left( \frac{2g}{L_2} + \frac{m_2 RA}{\rho L_2 T_h B_2^2} + \frac{m_3 RA}{\rho L_2 T_c B_3^2} \right) h_2 - \frac{m_2 RA}{\rho L_2 T_c B_3^2} h_1 - \frac{m_3 RA}{\rho L_2 T_h B_3^2} h_3 = 0, \quad (30)$$

$$\ddot{h}_3 + \frac{32\mu}{\rho d^2} \dot{h}_3 + \left( \frac{2g}{L_3} + \frac{m_3 RA}{\rho L_3 T_h B_3^2} + \frac{m_1 RA}{\rho L_3 T_c B_1^2} \right) h_3 - \frac{m_1 RA}{\rho L_3 T_h B_1^2} h_1 - \frac{m_3 RA}{\rho L_3 T_c B_3^2} h_2 = 0. \quad (31)$$

#### 4. Analysis of TDTASO with water column resonators

In this section, the onset criteria of TDTASOs are assessed based on the control theory [26]. The specifications of a prototype TDTASO constructed at Shiraz University of Technology is used in this section for further investigation of the onset criteria (see Table 1).

Table 1. Initial parameters of the prototype TDTASO

Parameter	Value	Parameter	Value
$d$	0.019 (m)	$L_i$	0.76 (m)
$A$	$2.83 \times 10^{-4}$ (m <sup>2</sup> )	$\mu$	$1.002 \times 10^{-3}$ (N s/m <sup>2</sup> )
$\rho$	997 (kg/m <sup>3</sup> )	$T_h$	200 (°C)
$R$	287 (N m/kg K)	$T_c$	20 (°C)
$m$	$2.1 \times 10^{-4}$ (kg)	$V_{c0}$	$9.07 \times 10^{-5}$ (m <sup>3</sup> )
$L$	1.4 (m)	$V_{h0}$	$9.07 \times 10^{-5}$ (m <sup>3</sup> )

In the following subsections, the oscillator dynamics is first expressed in the state-space and a new regulator-like system is proposed to justify the oscillator performance. Then, the onset temperature difference of the TDTASO is investigated corresponding to different geometries of the water columns. Next, the sensitivity of the oscillator to the consistency of the water column length in the U-tube resonators is investigated. Furthermore, the influence of the water column length and diameter on the instability of the oscillator are investigated.

##### 4.1. Applying modern control theory to the TDTASO with water column resonators

The modern control theory relies on the state-space representation of dynamical systems. Consequently, the state-space model (i.e., Eq. (32)) of the considered TDTASO system must first be acquired. Therefore, using Eqs. (10)–(12) and considering the state vector as  $\begin{bmatrix} h_1 & \dot{h}_1 & h_2 & \dot{h}_2 & h_3 & \dot{h}_3 \end{bmatrix}^T$ , the dynamic equations of the TDTASO system can be represented in the form of state-space as follows

$$\dot{\mathbf{x}} = \mathbf{A} \mathbf{x} + \mathbf{B} \mathbf{u}, \quad (32)$$

$$\begin{aligned}
 \begin{bmatrix} \dot{h}_1 \\ \ddot{h}_1 \\ \dot{h}_2 \\ \ddot{h}_2 \\ \dot{h}_3 \\ \ddot{h}_3 \end{bmatrix} &= \begin{bmatrix} 0 & 1 & 0 & 0 & 0 & 0 \\ -\frac{2g}{L_1} & -\frac{32\mu}{\rho d^2} & 0 & 0 & 0 & 0 \\ 0 & 0 & 0 & 1 & 0 & 0 \\ 0 & 0 & -\frac{2g}{L_2} & -\frac{32\mu}{\rho d^2} & 0 & 0 \\ 0 & 0 & 0 & 0 & 0 & 1 \\ 0 & 0 & 0 & 0 & -\frac{2g}{L_3} & -\frac{32\mu}{\rho d^2} \end{bmatrix} \begin{bmatrix} h_1 \\ \dot{h}_1 \\ h_2 \\ \dot{h}_2 \\ h_3 \\ \dot{h}_3 \end{bmatrix} \\
 &+ \begin{bmatrix} 0 & 0 & 0 & 0 & 0 & 0 \\ 0 & \frac{1}{\rho L_1} & 0 & 0 & 0 & 0 \\ 0 & 0 & 0 & 0 & 0 & 0 \\ 0 & 0 & 0 & \frac{1}{\rho L_2} & 0 & 0 \\ 0 & 0 & 0 & 0 & 0 & 0 \\ 0 & 0 & 0 & 0 & 0 & \frac{1}{\rho L_3} \end{bmatrix} \mathbf{u}, \tag{33}
 \end{aligned}$$

where

$$\mathbf{u} = -\mathbf{K} \mathbf{x} = - \begin{bmatrix} 0 \\ P_2 - P_1 \\ 0 \\ P_3 - P_2 \\ 0 \\ P_1 - P_3 \end{bmatrix}, \tag{34}$$

$$\mathbf{u} = \begin{bmatrix} 0 & 0 & 0 & 0 & 0 & 0 \\ \frac{m_1 RA}{\rho L_1 T_h B_1^2} + \frac{m_2 RA}{\rho L_1 T_c B_2^2} & 0 & -\frac{m_2 RA}{\rho L_1 T_h B_2^2} & 0 & -\frac{m_1 RA}{\rho L_1 T_c B_1^2} & 0 \\ 0 & 0 & 0 & 0 & 0 & 0 \\ -\frac{m_2 RA}{\rho L_2 T_c B_2^2} & 0 & \frac{m_2 RA}{\rho L_2 T_h B_2^2} + \frac{m_3 RA}{\rho L_2 T_c B_3^2} & 0 & -\frac{m_3 RA}{\rho L_2 T_h B_3^2} & 0 \\ 0 & 0 & 0 & 0 & 0 & 0 \\ -\frac{m_1 RA}{\rho L_3 T_h B_1^2} & 0 & -\frac{m_3 RA}{\rho L_3 T_c B_3^2} & 0 & \frac{m_3 RA}{\rho L_3 T_h B_3^2} + \frac{m_1 RA}{\rho L_3 T_c B_1^2} & 0 \end{bmatrix} \begin{bmatrix} h_1 \\ \dot{h}_1 \\ h_2 \\ \dot{h}_2 \\ h_3 \\ \dot{h}_3 \end{bmatrix}. \tag{35}$$

Manipulating the obtained state space model (i.e., Eqs. (33) and (35)), the similarity of the considered TDTASO to a regulator system in modern control theory is revealed. In fact, this latest finding is an important contribution of this article. As seen in Eq. (34), the pressure dynamics act as physical feedback in the

dynamic system. The block diagram of the TDTASO (Eqs. (32)–(35)) is shown in Fig. 6, which is a physical regulator defined in modern control theory.

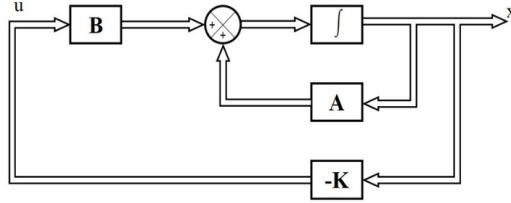


Fig. 6. Block diagram of the TDTASO (i.e. a regulator system)

Finally, the overall closed-loop state-space model of the TDTASO system is acquired by substituting Eq. (35) into Eq. (33) as:

$$\begin{bmatrix} \dot{h}_1 \\ \ddot{h}_1 \\ \dot{h}_2 \\ \ddot{h}_2 \\ \dot{h}_3 \\ \ddot{h}_3 \end{bmatrix} = \begin{bmatrix} 0 & 1 & 0 & 0 \\ \frac{2g}{L_1} - \frac{m_1 RA}{\rho L_1 T_h B_1^2} - \frac{m_2 RA}{\rho L_1 T_c B_2^2} & -\frac{32\mu}{\rho d^2} & \frac{m_2 RA}{\rho L_1 T_h B_2^2} & 0 \\ 0 & 0 & 0 & 1 \\ \frac{m_2 RA}{\rho L_2 T_c B_2^2} & 0 & -\frac{2g}{L_2} - \frac{m_2 RA}{\rho L_2 T_h B_2^2} - \frac{m_3 RA}{\rho L_2 T_c B_3^2} & -\frac{32\mu}{\rho d^2} \\ 0 & 0 & 0 & 0 \\ \frac{m_1 RA}{\rho L_3 T_h B_1^2} & 0 & \frac{m_3 RA}{\rho L_3 T_c B_3^2} & 0 \\ 0 & 0 & 0 & 0 \\ \frac{m_1 RA}{\rho L_1 T_c B_1^2} & 0 & 0 & 0 \\ 0 & 0 & 0 & 0 \\ \frac{m_3 RA}{\rho L_2 T_h B_3^2} & 0 & 0 & 0 \\ 0 & 1 & 0 & 0 \\ \frac{2g}{L_3} - \frac{m_3 RA}{\rho L_3 T_h B_3^2} - \frac{m_1 RA}{\rho L_3 T_c B_1^2} & -\frac{32\mu}{\rho d^2} & 0 & 0 \end{bmatrix} \begin{bmatrix} h_1 \\ \dot{h}_1 \\ h_2 \\ \dot{h}_2 \\ h_3 \\ \dot{h}_3 \end{bmatrix}. \quad (36)$$

It is clear that the closed-loop poles of the TDTASO system are the eigenvalues of the state matrix in Eq. (36). Subsequently, the eigenvalues of the considered regulator system (i.e., TDTASO) can be found based on the following characteristic equation

$$\det(\lambda I - A) = \lambda^6 + u_1 \lambda^5 + u_2 \lambda^4 + u_3 \lambda^3 + u_4 \lambda^2 + u_5 \lambda + u_6 = 0, \quad (37)$$

where  $u_i$  are functions of the oscillator parameters. The values of  $u_i$  are given in Appendix A.

## 4.2. Predicting onset temperature difference of the TDTASO

In the previous subsection, the similarity of the TDTASO to a regulator system was revealed. Accordingly, the positions of the closed-loop poles of the TDTASO system can be calculated based on the state feedback gain matrix  $\mathbf{K}$  (see Eqs. (34) and (35)) in which different oscillator parameters such as hot and cold gas temperatures can be seen. In this subsection, the onset temperature difference of the TDTASO for various water column lengths and diameters is investigated based on the eigenvalues of state matrix of the closed-loop regulator system and root locus technique. It's clear that the dominant closed-loop poles of the oscillator cross the imaginary axis to the right-hand side of the s-plane when the temperature of the system reaches the onset temperature difference. Investigating the onset temperature difference is done taking into consideration different water column lengths of 0.36, 0.44, 0.52, 0.6, 0.68 and 0.76 meters at different U-tube diameters of 0.019 and 0.025 meters. Fig. 7 and Fig. 8 demonstrate the root locus plots for varying values of onset temperature difference ranging from  $57^{\circ}\text{C}$  to  $407^{\circ}\text{C}$  corresponding to the water column length of 0.36 m at water column diameters of 0.019 m and 0.025 m, respectively. The graphs show that the dominant closed-loop poles move toward the right-hand side of the s-plane by increasing the temperature difference and cross the imaginary axis at temperature difference of  $183^{\circ}\text{C}$  and  $171^{\circ}\text{C}$  (i.e., onset temperature difference) corresponding to the water column diameters of 0.019 m and 0.025 m, respectively. It is worth noting that when the imaginary part of the dominant closed-loop poles of the oscillator increases the oscillator frequency will be increased while the increase of real component of the poles results in enhancing the oscillator work [27]. Accordingly, increasing the temperature difference beyond the required onset temperature causes the oscillator frequency and output power to be augmented.

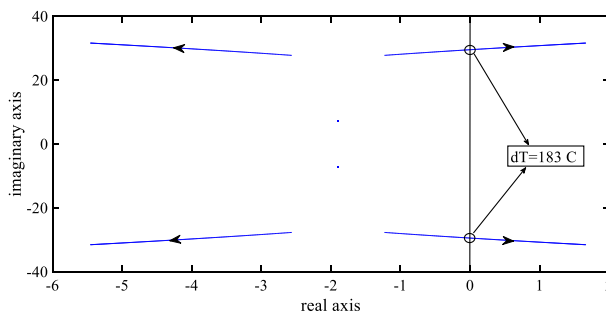


Fig. 7. Root locus diagram for varying value of onset temperature difference within the range  $57^{\circ}\text{C}$ – $407^{\circ}\text{C}$  for water column of 0.36 m and U-tube diameter of 0.019 m once  $T_c = 20^{\circ}\text{C}$

More numerical results on the onset temperature difference for different dimensions of the water column resonators are given in Table 2 using the proposed control-based mathematical scheme.

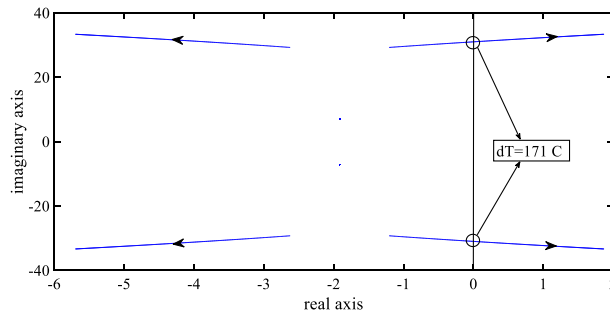


Fig. 8. Root locus diagram for varying value of onset temperature difference within the range  $57^{\circ}\text{C}$ – $407^{\circ}\text{C}$  for water column of 0.36 m and U-tube diameter of 0.025 m once  $T_c = 20^{\circ}\text{C}$

Table 2. The simulated onset temperature difference of the TDTASO for different dimensions of the water column resonators

Water column length $L_i$ (m)	Onset temperature difference ( $^{\circ}\text{C}$ )	
	$d = 0.019$ m	$d = 0.025$ m
0.76	160	152
0.68	166	158
0.60	171	164
0.52	174	168
0.44	175	170
0.36	183	171

As seen in Table 2, increasing the length of the water column in U-tube resonators reduces the onset temperature difference of the TDTASO. This recent finding can be attributed to the fact that reducing the water column length results in increasing the initial volume and mass of the gas column located above the water level.

### 4.3. Investigating the oscillator sensitivity to mismatched water column lengths in U-tube resonators

An important question may arise about the allowable discrepancy among the water column lengths in the three U-tube resonators of the proposed oscillator. In this subsection, this important question is responded and the robustness of the TDTASO against the mentioned challenge is investigated numerically. Thus, the length of water columns in two of the U-tubes keeps constant at 0.48 m while the length of water column changes from 0.34 m to 0.8 m in the third U-tube. This investigation is carried out considering two water column diameters of 0.019 m and 0.025 m, respectively. The root locus diagrams pertaining to the variations of the water column length in one of the oscillator's stage are depicted in Fig. 9 and Fig. 10 for resonator diameters of 0.019 m and 0.025 m, respectively.

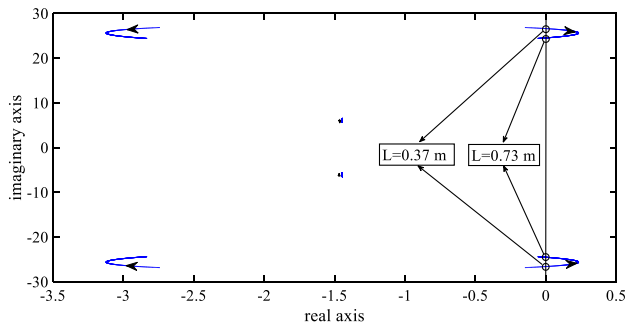


Fig. 9. Root locus diagram for varying values of the water column length in one of the U-tube resonators from 0.34 m to 0.8 m (length of other resonators = 0.48 m, diameter = 0.019 m,  $T_h = 200^\circ\text{C}$ , and  $T_c = 20^\circ\text{C}$ )

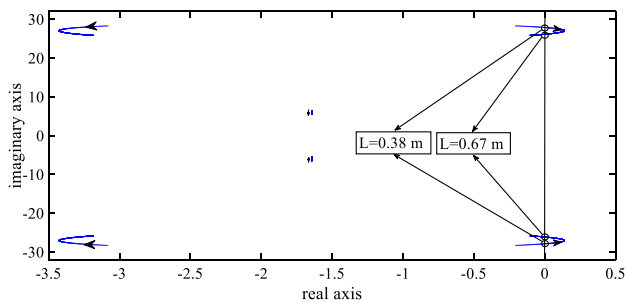


Fig. 10. Root locus diagram for varying values of the water column length in one of the U-tube resonators from 0.34 m to 0.80 m (length of other resonators = 0.48 m, diameter = 0.025 m,  $T_h = 200^\circ\text{C}$ , and  $T_c = 20^\circ\text{C}$ )

The obtained numerical results reveal that just for a specific range of the water column length in one of the U-tubes the root loci concerning the dominant poles are placed on the right hand side of the s-plane. It means that the inconsistency of the water columns lengths inside the U-tube resonators considerably affects the overall instability of the equilibrium state of the considered TDTASO. As seen in the root locus diagrams, the instability state of the oscillator occurs once the considered water column length ranges from 0.37 m and 0.73 m for the diameter of 0.019 m and from 0.38 m and 0.67 m for the diameter of 0.025 m.

#### 4.4. Predicting onset conditions based on the matched water column lengths in U-tube resonators

In this subsection, assuming the same water column lengths within all U-tube resonators (i.e., matched water columns), the effect of variations of the water column length (ranging from 0.15 m to 1.2 m at both diameters of 0.019 m and 0.025 m) on the oscillator instability at the startup state is investigated based on the root locus diagrams represented in Fig. 11 and Fig. 12. As can be seen, the TDTASO oscillator starts to operate once the water column lengths achieve 0.22 m

and 0.25 m for U-tube diameters of 0.019 m and 0.025 m, respectively. Moreover, increasing the water column length beyond the mentioned values results in reducing the operating frequency and increasing the output work of the oscillator.

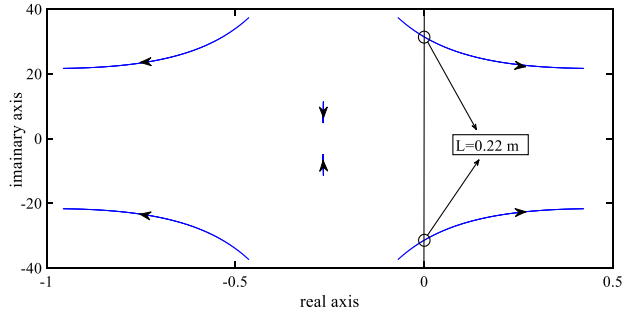


Fig. 11. Root locus diagram for varying values of water column length ranging from 0.15 m to 1.2 m for U-tube diameter of 0.019 m ( $T_c = 20^\circ\text{C}$  and  $T_h = 200^\circ\text{C}$ )

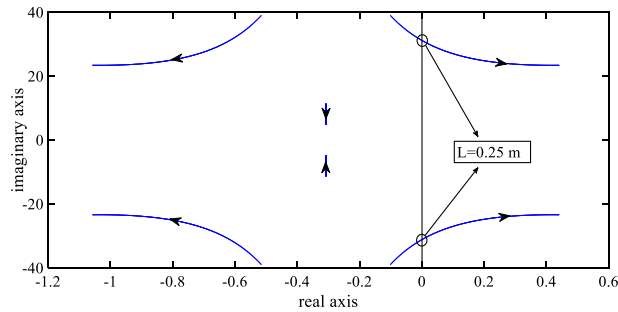


Fig. 12. Root locus diagram for varying values of water column length ranging from 0.15 m to 1.2 m for U-tube diameter of 0.025 m ( $T_c = 20^\circ\text{C}$  and  $T_h = 200^\circ\text{C}$ )

#### 4.5. Predicting onset conditions based on matched water column diameters in U-tube resonators

In this subsection, the influence of U-tube diameter on the instability of the TDTASO is investigated. The investigation is done considering the diameter variation within the range [0.01 m–0.03 m] for water column lengths of 0.36 m and 0.76 m. The root locus diagrams are shown in Fig. 13 and Fig. 14.

It is interesting to note that the oscillator operates using a specific range of water column diameter, i.e., 0.0136 m–0.0294 m for water column length of 0.36 m and 0.0152 m–0.0289 m for water column of 0.76 m. In addition, there is an optimum value for the resonator diameter in which a maximum power can be picked up (i.e., optimum diameter of 0.0204 m for water column length of 0.36 m and diameter 0.0213 m for water column length of 0.76 m).



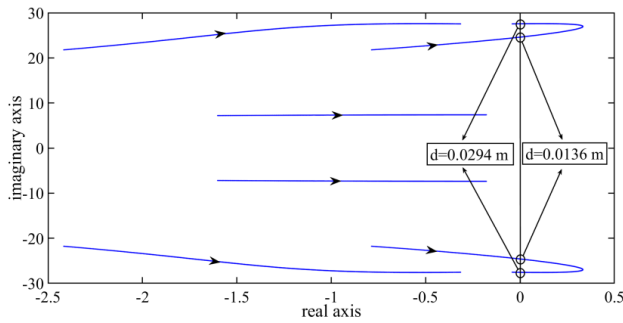


Fig. 13. Root locus diagram for varying values of water column diameter ranging from 0.01 m to 0.03 m for water column length of 0.36 m ( $T_c = 20^\circ\text{C}$  and  $T_h = 200^\circ\text{C}$ )

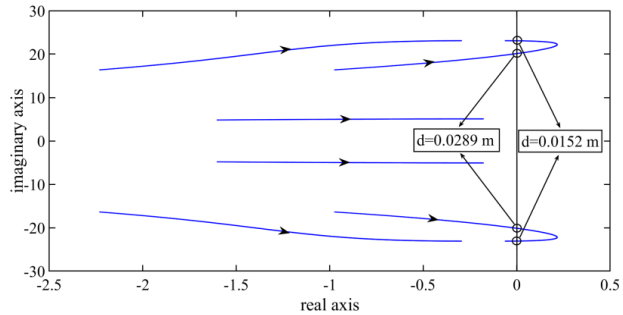


Fig. 14. Root locus diagram for varying values of water column diameter ranging from 0.01 m to 0.03 m for water column length of 0.76 m ( $T_c = 20^\circ\text{C}$  and  $T_h = 200^\circ\text{C}$ )

## 5. Experimental study

In this section, a prototype TDTASO with water column resonators (see Fig. 15) is developed and tested so as to verify the proposed mathematical model as well as the simulation results. The considered values of design parameters were previously given in Table 1. In the experimental rig, the K-type skinned thermocouple is used to measure the hot and cold gas temperatures within the heat exchangers. An MPXV7002 module is utilized to measure working gas pressure and the oscillator frequency (using fast Fourier transform of the pressure signal) at startup moment. An NI-USB6009 data acquisition system with 14-bit resolution (for analog input channels) is employed to log the measured data. The experimental stand diagram is shown in Fig. 16. In the following, the onset temperature difference of the TDTASO for a range of water column length is evaluated. Then, the discrepancy between the working frequency of the oscillator and the natural frequency of each water column inside the U-tube resonators is revealed through experiment. At the end, the practical sensitivity of the oscillator to the mismatched water column lengths in the U-shaped resonators is investigated experimentally.

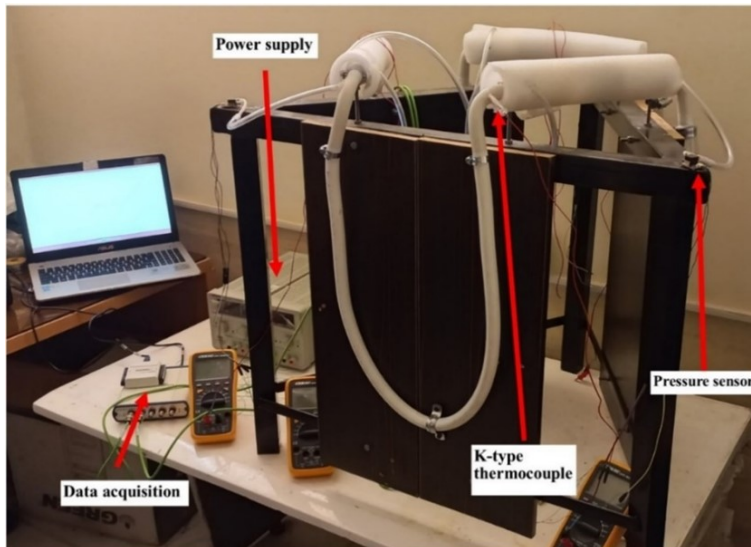


Fig. 15. The developed three-stage double-acting thermoacoustic Stirling oscillator with water piston

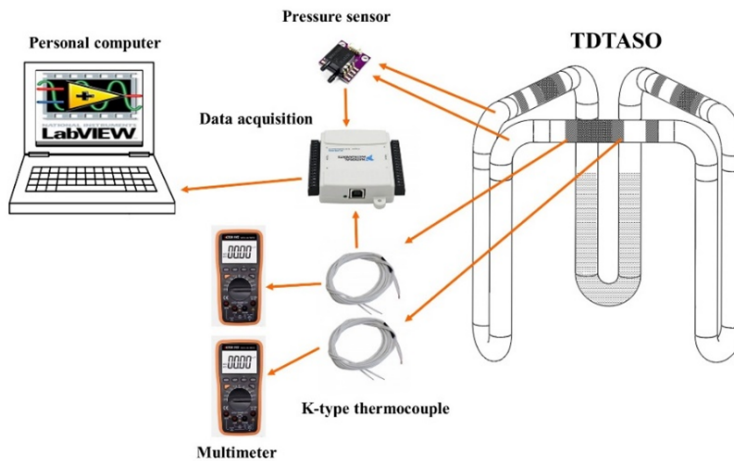


Fig. 16. The experimental stand diagram

### 5.1. Measurement of onset temperature difference corresponding to various resonator dimensions

The onset temperature difference is measured with the k-type thermocouples that are placed at both sides of the regenerator sections without contacting the inside walls of the oscillator. The onset temperature difference is found for different water column lengths of 0.36, 0.44, 0.52, 0.6, 0.68 and 0.76 m corresponding to different U-tube diameters of 0.019 m and 0.025 m. As mentioned previously, the

onset temperature difference is the value of the temperature difference at which the oscillator starts to operate. So, for diagnosing the mentioned unstable status, the pressure and temperature signals obtained from the pressure and temperature sensors are utilized. In other words, the pressure and temperature of the working gas within the hot and cold heat exchangers are measured simultaneously. Thus, the onset temperature difference is one at which the pressure signal shows unstable

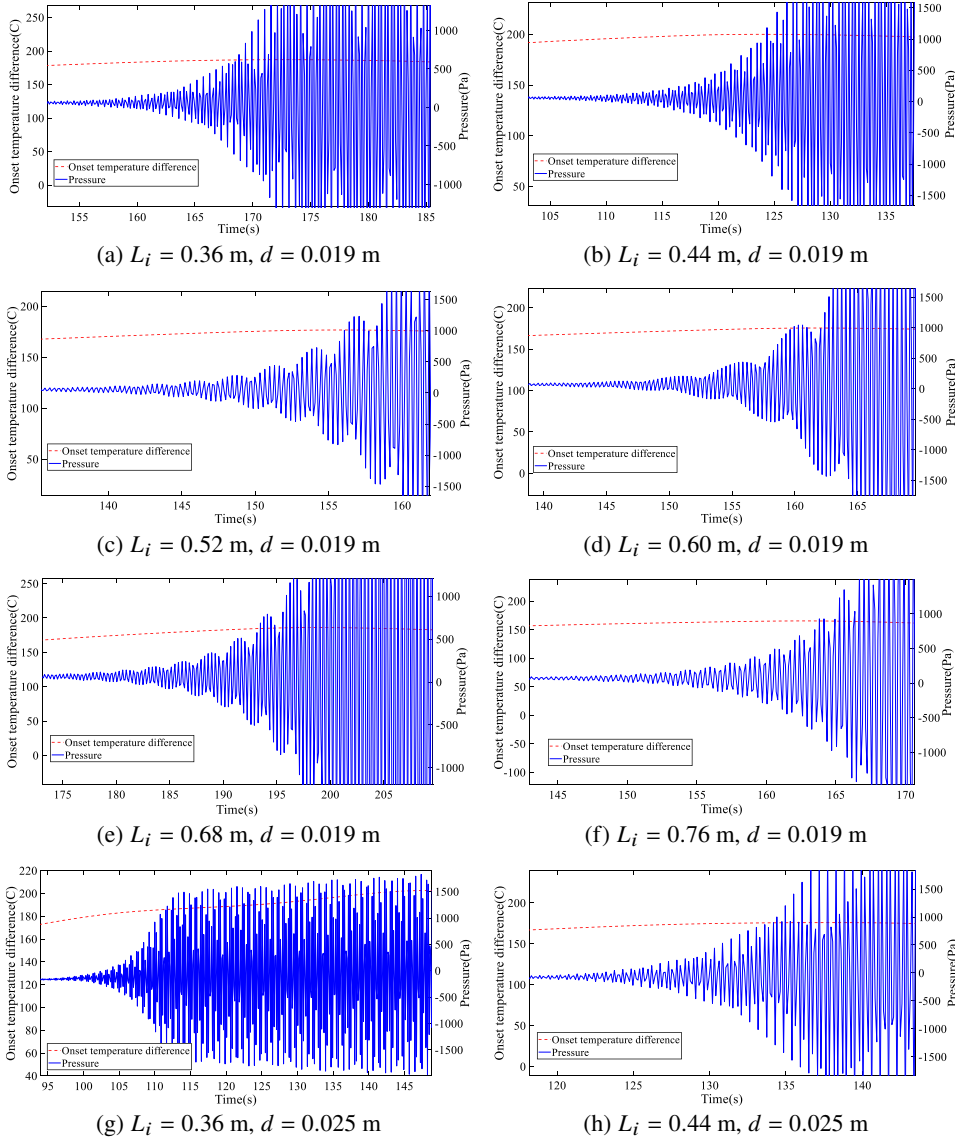


Fig. 17. Experimental results of onset temperature difference and gas pressure for different water column length ( $L_i$ ) and tube diameter ( $d$ )

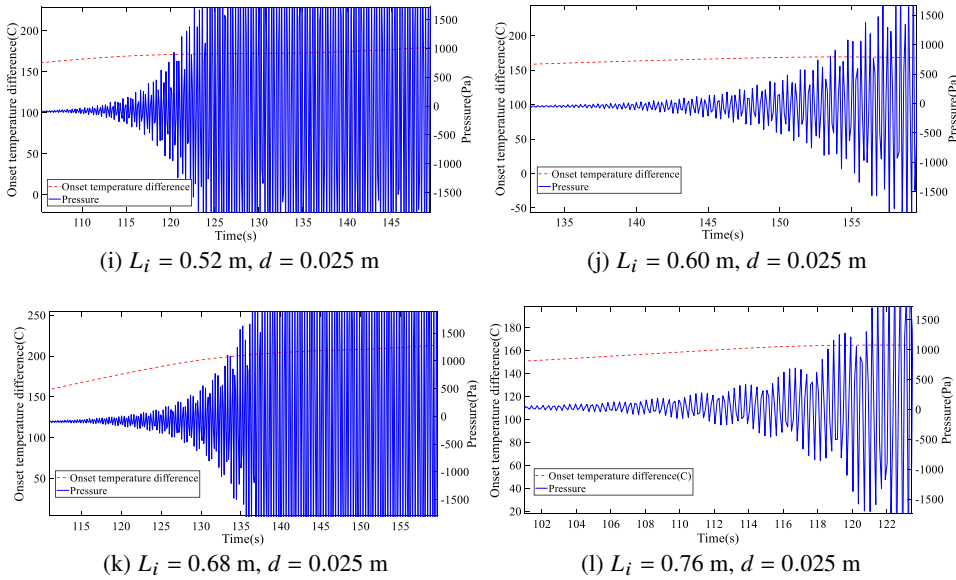


Fig. 17. Experimental results of onset temperature difference and gas pressure for different water column length ( $L_i$ ) and tube diameter ( $d$ )

dynamics. Figs. 17a–17l demonstrate the measured instantaneous pressure and temperatures for different dimensions of the water column resonators.

As can be inferred from Figs. 17a–17l, the onset temperature difference decreases with increasing the water column length, which affirms the obtained simulation results. Table 3 presents a comparison between experimental and simulation data of the onset temperature difference.

Table 3. Comparison between experimental and simulation data of onset temperature difference

Water column length $L_i$ (m)	Simulation data of onset temperature difference ( $^{\circ}$ C)		Experimental data of onset temperature difference ( $^{\circ}$ C)	
	$d = 0.019$ m	$d = 0.025$ m	$d = 0.019$ m	$d = 0.025$ m
0.76	162	157	157	151
0.68	164	158	168	159
0.60	166	160	166	158
0.52	170	163	167	160
0.44	176	167	172	166
0.36	183	172	178	173

## 5.2. Operating frequency of the oscillator versus resonant frequency of water column resonators

One of the important parameters of the TDTASO considered in this investigation is the working frequency of the oscillator. It is now questionable whether

the system operating frequency is the same as the resonant frequency of the water column resonators or not. If one compares Eqs. (10)–(12) to Eqs. (29)–(31), it can be easily understood that the stiffness terms are not the same in the U-tube resonator dynamics defined by Eqs. (10)–(12) and the closed-loop dynamics of the oscillator defined by Eqs. (29)–(31). It means that the operating frequency would be different from the resonant frequency of the U-tube resonators due to the effect of gas springs used between the two adjacent water columns. In this subsection, this significant issue is responded experimentally. To check this issue, the natural frequency of the U-shaped tube for three number of water column lengths is found and compared to the working frequency obtained from experimental data. The outcomes are shown in Table 4.

Table 4. Comparison between natural frequency and working frequency of the TPDTSEWP

Water column length $L_i$ (m)	Natural frequency of water columns (Hz)	Working frequency of the oscillator (Hz)
0.52	0.81	3.14
0.44	1	3.34
0.36	1.1	3.55

Table 4 shows that the operating frequency of the oscillator is greater than the natural frequency of the water columns inside the U-tubes, which can be attributed to the addition of the gas springs between the water columns.

### 5.3. Experimental evaluation of the oscillator sensitivity to inconsistency of water column lengths

To investigate the sensitivity of the oscillator to mismatched lengths of water columns in the U-tube resonators experimentally, the lengths of water columns in two of the U-tube resonators remain constant at 0.48 m while the length of the water column in just one of the U-tube is shifted. The practical results show that the TDTASO can operate in a specific range of the mismatched water column length i.e., 0.36 m–0.72 m corresponding to the tube diameter of 0.019 m and 0.4 m–0.68 m corresponding to 0.025 m of tube diameter. Subsequently, the operating frequencies of the oscillator corresponding to different mismatched water column lengths are found and given in Table 5. It can be observed that decreasing the water column length lower than the matched length (i.e., 0.48 m) increases to operating frequency while increasing the water column length more than the matched length reduces the operating frequency as well.

Fig. 18 and Fig. 19 show a comparison between the working frequency corresponding to the mismatched water column length obtained from experimental and simulation studies for 0.019 m and 0.025 m of tube diameter, respectively. It is obvious that the working frequency decreases as the mismatched water column length increases.

Table 5. Operating frequency of the TDTASO with a mismatched water column length

Water column length of mismatched resonator $L_i$ (m)	Operating frequency (Hz)	
	$d = 0.019$ m	$d = 0.025$ m
0.34	–	–
0.36	3.29	–
0.40	3.28	3.66
0.44	3.24	3.6
0.48*	3.23	3.57
0.52	3.19	3.54
0.56	3.19	3.5
0.60	3.14	3.5
0.64	3.14	3.47
0.68	3.07	3.47
0.72	3.09	–
0.74	–	–

\* Matched water column length, – Not applicable

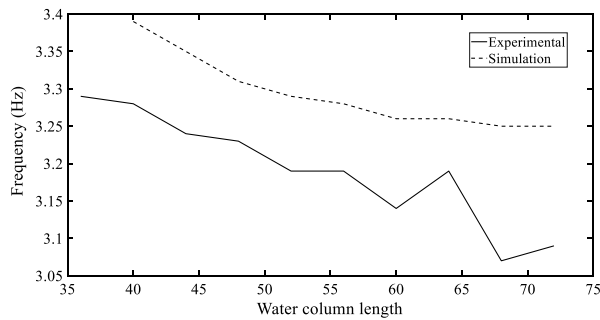


Fig. 18. Experimental versus simulated working frequency of the TDTASO for 0.019 m of tube diameter for varying values of mismatched water column length in one of the U-tube

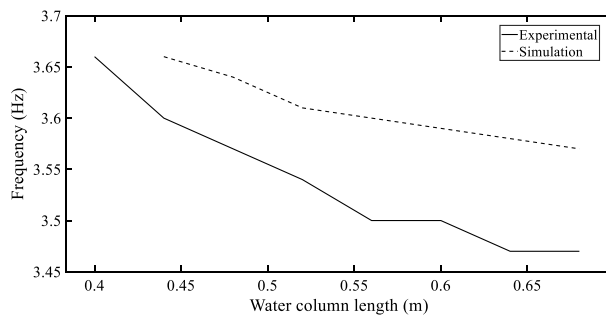


Fig. 19. Experimental versus simulated working frequency of the TDTASO for 0.025 m of tube diameter for varying values of mismatched water column length in one of the U-tube

## 6. Conclusions

In this work, a three-phase double-acting thermoacoustic Stirling oscillator with water column resonators was first modeled and analyzed based on a novel control-based design approach incorporating the conventional Schmidt's theory. Then, the applicability of the proposed mathematical scheme to design a thermoacoustic Stirling oscillator was further affirmed through experiment. It was shown that according to modern control theory, the TDTASO with water pistons was a physical feedback regulator and therefore, designing of such systems can be done through the powerful techniques of modern control. The obtained outcomes revealed that by increasing the length of the matched water columns, the onset temperature difference was reduced and at a specific length of the matched water columns, the oscillator with a larger resonator diameter operated at a lower onset temperature difference. Accordingly, the onset temperature difference decreased about 11% for 0.019 m of tube diameter and about 8% for 0.025 m of tube diameter once the matched water column lengths increased from 0.36 m to 0.76 m. Besides, increasing the diameter of the water column resonators from 0.019 m to 0.025 m reduced the oscillator onset temperature difference by 5%. Next, the sensitivity of such a three-phase oscillator to the inconsistency of the length of the water columns was investigated. It was found that the TSTASE system was robust to variation of the water column length in one of the resonators while the rest of the water column lengths were unchanged. Accordingly, for the U-tube diameter of 0.019 m, the oscillator operated at a specific range of mismatched water column length, i.e., 0.36 m–0.72 m while for the diameters of 0.025 m the allowable range of the mismatched water column length was 0.40 m–0.68 m. The existence of some discrepancies between the oscillator operating frequency and the resonant frequency of the U-shaped resonators was another significant outcome of this work. It was shown that the oscillator operating frequency was higher than the resonant frequency of the U-shaped resonators. Stability investigation of the presented thermoacoustic systems with nonlinear characteristic based on the stability theorems will be studied in the future works.

### A. Appendix

The values of parameters  $u_i$  given in Eq. (37) can be calculated as follows:

$$u_1 = \frac{96\mu}{\rho d^2}, \quad (38)$$

$$u_2 = \frac{3072\mu^2}{\rho^2 d^4} + \frac{2g}{L_1} + \frac{2g}{L_2} + \frac{2g}{L_3} + \frac{m_1 RA}{\rho L_1 T_h B_1^2} + \frac{m_1 RA}{\rho L_3 T_c B_1^2} + \frac{m_2 RA}{\rho L_2 T_h B_2^2} + \frac{m_2 RA}{\rho L_1 T_c B_2^2} + \frac{m_3 RA}{\rho L_3 T_h B_3^2} + \frac{m_3 RA}{\rho L_2 T_c B_3^2}, \quad (39)$$

$$\begin{aligned}
 u_3 = & \frac{128\mu g}{\rho d^2 L_1} + \frac{128\mu g}{\rho d^2 L_2} + \frac{128\mu g}{\rho d^2 L_3} + \frac{64\mu m_1 RA}{\rho^2 d^2 L_1 T_h B_1^2} + \frac{64\mu m_1 RA}{\rho^2 d^2 L_3 T_c B_1^2} + \frac{64\mu m_2 RA}{\rho^2 d^2 L_2 T_h B_2^2} \\
 & + \frac{64\mu m_2 RA}{\rho^2 d^2 L_1 T_c B_2^2} + \frac{64\mu m_3 RA}{\rho^2 d^2 L_3 T_h B_3^2} + \frac{64\mu m_3 RA}{\rho^2 d^2 L_2 T_c B_3^2} + \frac{32768\mu^3}{\rho^3 d^6}, \quad (40)
 \end{aligned}$$

$$\begin{aligned}
 u_4 = & \frac{4g^2}{L_1 L_2} + \frac{4g^2}{L_1 L_3} + \frac{4g^2}{L_2 L_3} + \frac{2048\mu^2 g}{\rho^2 d^4 L_2} + \frac{2048\mu^2 g}{\rho^2 d^4 L_3} + \frac{2048\mu^2 g}{\rho^2 d^4 L_1} \\
 & + \frac{1024\mu^2 m_3 RA}{\rho^3 d^4 L_3 T_h B_3^2} + \frac{1024\mu^2 m_1 RA}{\rho^3 d^4 L_3 T_c B_1^2} + \frac{1024\mu^2 m_1 RA}{\rho^3 d^4 L_1 T_h B_1^2} + \frac{1024\mu^2 m_2 RA}{\rho^3 d^4 L_1 T_c B_2^2} \\
 & + \frac{1024\mu^2 m_2 RA}{\rho^3 d^4 L_2 T_h B_2^2} + \frac{1024\mu^2 m_3 RA}{\rho^3 d^4 L_2 T_c B_3^2} + \frac{m_1 m_3 R^2 A^2}{\rho^2 L_1 L_3 T_h^2 B_1^2 B_3^2} + \frac{m_1 m_3 R^2 A^2}{\rho^2 L_2 L_3 T_c^2 B_1^2 B_3^2} \\
 & + \frac{m_1 m_2 R^2 A^2}{\rho^2 L_1 L_3 T_c^2 B_1^2 B_2^2} + \frac{m_2 m_3 R^2 A^2}{\rho^2 L_1 L_2 T_c^2 B_2^2 B_3^2} + \frac{m_2 m_3 R^2 A^2}{\rho^2 L_2 L_3 T_h^2 B_2^2 B_3^2} \\
 & + \frac{m_1 m_2 R^2 A^2}{\rho^2 L_1 L_2 T_h^2 B_1^2 B_2^2} + \frac{m_2 m_3 R^2 A^2}{\rho^2 L_1 L_3 T_c T_h B_2^2 B_3^2} + \frac{m_1 m_2 R^2 A^2}{\rho^2 L_2 L_3 T_c T_h B_1^2 B_2^2} \\
 & + \frac{m_1 m_3 R^2 A^2}{\rho^2 L_1 L_2 T_c T_h B_1^2 B_3^2} + \frac{2m_1 RA g}{\rho L_2 L_3 T_c B_1^2} + \frac{2m_3 RA g}{\rho L_2 L_3 T_h B_3^2} + \frac{2m_2 RA g}{\rho L_1 L_2 T_c B_2^2} \\
 & + \frac{2m_1 RA g}{\rho L_1 L_2 T_h B_1^2} + \frac{2m_3 RA g}{\rho L_2 L_3 T_c B_3^2} + \frac{2m_2 RA g}{\rho L_2 L_3 T_h B_2^2} + \frac{2m_3 RA g}{\rho L_1 L_2 T_c B_3^2} + \frac{2m_3 RA g}{\rho L_1 L_3 T_h B_3^2} \\
 & + \frac{2m_1 RA g}{\rho L_1 L_3 T_c B_1^2} + \frac{2m_2 RA g}{\rho L_1 L_2 T_h B_2^2} + \frac{2m_2 RA g}{\rho L_1 L_3 T_c B_2^2} + \frac{2m_1 RA g}{\rho L_1 L_3 T_h B_1^2}, \quad (41)
 \end{aligned}$$

$$\begin{aligned}
 u_5 = & \frac{128\mu g^2}{\rho d^2 L_1 L_2} + \frac{128\mu g^2}{\rho d^2 L_1 L_3} + \frac{128\mu g^2}{\rho d^2 L_2 L_3} + \frac{64\mu m_3 RA g}{\rho^2 d^2 L_2 L_3 T_h B_3^2} + \frac{64\mu m_2 RA g}{\rho^2 d^2 L_1 L_2 T_c B_2^2} \\
 & + \frac{64\mu m_2 RA g}{\rho^2 d^2 L_2 L_3 T_h B_2^2} + \frac{64\mu m_3 RA g}{\rho^2 d^2 L_2 L_3 T_c B_3^2} + \frac{64\mu m_2 RA g}{\rho^2 d^2 L_1 L_3 T_c B_2^2} + \frac{64\mu m_1 RA g}{\rho^2 d^2 L_2 L_3 T_c B_1^2} \\
 & + \frac{64\mu m_1 RA g}{\rho^2 d^2 L_1 L_2 T_h B_1^2} + \frac{64\mu m_1 RA g}{\rho^2 d^2 L_1 L_3 T_c B_1^2} + \frac{64\mu m_1 RA g}{\rho^2 d^2 L_1 L_3 T_h B_1^2} + \frac{64\mu m_3 RA g}{\rho^2 d^2 L_1 L_2 T_c B_3^2} \\
 & + \frac{64\mu m_3 RA g}{\rho^2 d^2 L_1 L_3 T_h B_3^2} + \frac{64\mu m_2 RA g}{\rho^2 d^2 L_1 L_2 T_h B_2^2} + \frac{32\mu m_1 m_2 R^2 A^2}{\rho^3 d^2 L_1 L_2 T_h^2 B_1^2 B_2^2} \\
 & + \frac{32\mu m_1 m_2 R^2 A^2}{\rho^3 d^2 L_1 L_3 T_c^2 B_1^2 B_2^2} + \frac{32\mu m_1 m_3 R^2 A^2}{\rho^3 d^2 L_2 L_3 T_c^2 B_1^2 B_3^2} + \frac{32\mu m_2 m_3 R^2 A^2}{\rho^3 d^2 L_1 L_2 T_c^2 B_2^2 B_3^2} \\
 & + \frac{32\mu m_1 m_2 R^2 A^2}{\rho^3 d^2 L_2 L_3 T_c T_h B_1^2 B_2^2} + \frac{32\mu m_1 m_3 R^2 A^2}{\rho^3 d^2 L_1 L_2 T_c T_h B_1^2 B_3^2} + \frac{32\mu m_2 m_3 R^2 A^2}{\rho^3 d^2 L_2 L_3 T_h^2 B_2^2 B_3^2} \\
 & + \frac{32\mu m_2 m_3 R^2 A^2}{\rho^3 d^2 L_1 L_3 T_c T_h B_2^2 B_3^2} + \frac{32\mu m_1 m_3 R^2 A^2}{\rho^3 d^2 L_1 L_3 T_h^2 B_1^2 B_3^2}, \quad (42)
 \end{aligned}$$



$$\begin{aligned}
 u_6 = & \frac{2m_1m_2R^2A^2g}{\rho^2L_1L_2L_3T_cT_hB_1^2B_2^2} + \frac{2m_1m_3R^2A^2g}{\rho^2L_1L_2L_3T_c^2B_1^2B_3^2} + \frac{2m_1m_2R^2A^2g}{\rho^2L_1L_2L_3T_h^2B_1^2B_2^2} \\
 & + \frac{2m_1m_2R^2A^2g}{\rho^2L_1L_2L_3T_c^2B_1^2B_2^2} + \frac{2m_1m_3R^2A^2g}{\rho^2L_1L_2L_3T_cT_hB_1^2B_3^2} + \frac{2m_2m_3R^2A^2g}{\rho^2L_1L_2L_3T_h^2B_2^2B_3^2} \\
 & + \frac{2m_1m_3R^2A^2g}{\rho^2L_1L_2L_3T_h^2B_1^2B_3^2} + \frac{2m_2m_3R^2A^2g}{\rho^2L_1L_2L_3T_cT_hB_2^2B_3^2} + \frac{2m_2m_3R^2A^2g}{\rho^2L_1L_2L_3T_c^2B_2^2B_3^2} \\
 & + \frac{4m_1RAg^2}{\rho L_1L_2L_3T_cB_1^2} + \frac{4m_2RAg^2}{\rho L_1L_2L_3T_hB_2^2} + \frac{4m_1RAg^2}{\rho L_1L_2L_3T_hB_1^2} \\
 & + \frac{4m_3RAg^2}{\rho L_1L_2L_3T_cB_3^2} + \frac{4m_2RAg^2}{\rho L_1L_2L_3T_cB_2^2} + \frac{4m_3RAg^2}{\rho L_1L_2L_3T_hB_3^2} + \frac{8g^3}{L_1L_2L_3}. \quad (43)
 \end{aligned}$$

### Acknowledgement

The authors would like to thank the Shiraz University of Technology for providing research facilities and supports.

### Data availability statement

The data that support the findings of this study are available from the corresponding author upon reasonable request.

### References

- [1] S. Zare and A. Tavakolpour-Saleh. Free piston Stirling engines: A review. *International Journal of Energy Research*, 44(7):5039–5070, 2020. doi: [10.1002/er.4533](https://doi.org/10.1002/er.4533).
- [2] S. Zare, A. Tavakolpour-Saleh, and M. Sangdani. Investigating limit cycle in a free piston Stirling engine using describing function technique and genetic algorithm. *Energy Conversion and Management*, 210:112706, 2020. doi: [10.1016/j.enconman.2020.112706](https://doi.org/10.1016/j.enconman.2020.112706).
- [3] G. Walker and J.R. Senft. *Free-Piston Stirling Engines*. Springer, 1985. doi: [10.1007/978-3-642-82526-2\\_2](https://doi.org/10.1007/978-3-642-82526-2_2).
- [4] S. Zare and A. Tavakolpour-Saleh. Applying particle swarm optimization to study the effect of dominant poles places on performance of a free piston Stirling engine. *Arabian Journal for Science and Engineering*, 44(6):5657–5669, 2019. doi: [10.1007/s13369-018-3677-1](https://doi.org/10.1007/s13369-018-3677-1).
- [5] S. Zare and A. Tavakolpour-Saleh. Modeling, construction, and testing of a diaphragm thermoacoustic Stirling engine. *Energy Conversion and Management*, 243:114394, 2021. doi: [10.1016/j.enconman.2021.114394](https://doi.org/10.1016/j.enconman.2021.114394).
- [6] P. Murti, A. Tkizawa, E. Shoji, and T. Biwa. Design guideline for multi-cylinder-type liquid-piston Stirling engine. *Applied Thermal Engineering*, 200:117635, 2022. doi: [10.1016/j.applthermaleng.2021.117635](https://doi.org/10.1016/j.applthermaleng.2021.117635).
- [7] S. Backhaus and G.W. Swift. A thermoacoustic-Stirling heat engine: Detailed study. *The Journal of the Acoustical Society of America*, 107(6):3148–3166, 2000. doi: [10.1121/1.429343](https://doi.org/10.1121/1.429343).
- [8] S. Backhaus and G.W. Swift. A thermoacoustic Stirling heat engine. *Nature*, 399(6734):335–338, 1999. doi: [10.1038/20624](https://doi.org/10.1038/20624).

- [9] C. Iniesta, J.L. Olazagoitia, J. Vinolas, and J. Aranceta. Review of travelling-wave thermoacoustic electric-generator technology. *Proceedings of the Institution of Mechanical Engineers, Part A: Journal of Power and Energy*, 232(7):940–957, 2018. doi: [10.1177/0957650918760627](https://doi.org/10.1177/0957650918760627).
- [10] T.W. Steiner, et al. High-efficiency natural gas fired 1 kWe thermoacoustic engine. *Applied Thermal Engineering*, 199:117548, 2021. doi: [10.1016/j.applthermaleng.2021.117548](https://doi.org/10.1016/j.applthermaleng.2021.117548).
- [11] E. Luo, H. Ling, W. Dai, and Y. Zhang. A high pressure-ratio, energy-focused thermoacoustic heat engine with a tapered resonator. *Chinese Science Bulletin*, 50(3):284–286, 2005. doi: [10.1007/BF02897541](https://doi.org/10.1007/BF02897541).
- [12] S. Zhang, L. Zhang, and E. Luo. Influence of asymmetric structure on performance of double-acting traveling-wave thermoacoustic engine with liquid piston. *Cryogenics*, 185:25–32, 2012. (in Chinese).
- [13] D.H. Li, L.M. Zhang, Z.H. Wu, and E. Luo. Numerical simulation and experimental investigation of a gas-liquid, double-acting traveling-wave thermoacoustic heat engine. *International Journal of Energy Research*, 37(15):1963–1970, 2013. doi: [10.1002/er.3060](https://doi.org/10.1002/er.3060).
- [14] K. Wang, S.R. Sanders, S. Dubey, F.H. Choo, and F. Duan. Stirling cycle engines for recovering low and moderate temperature heat: A review. *Renewable and Sustainable Energy Reviews*, 62:89–108, 2016. doi: [10.1016/j.rser.2016.04.031](https://doi.org/10.1016/j.rser.2016.04.031).
- [15] S. Zhang and E. Luo. The thermodynamic performance of a double-acting traveling-wave thermoacoustic engine with liquid-water piston. *International Journal of Green Energy*, 12(3):198–206, 2015. doi: [10.1080/15435075.2014.891522](https://doi.org/10.1080/15435075.2014.891522).
- [16] D. Li, Y. Chen, E. Luo, and Z. Wu. Study of a liquid-piston traveling-wave thermoacoustic heat engine with different working gases. *Energy*, 74:158–163, 2014. doi: [10.1016/j.energy.2014.05.034](https://doi.org/10.1016/j.energy.2014.05.034).
- [17] S. Tamura, H. Hyodo, and T. Biwa. Experimental and numerical analysis of a liquid-piston Stirling engine with multiple unit sections. *Japanese Journal of Applied Physics*, 58(1):017001, 2018. doi: [10.7567/1347-4065/aae930](https://doi.org/10.7567/1347-4065/aae930).
- [18] H. Hyodo, S. Tamura, and T. Biwa. A looped-tube traveling-wave engine with liquid pistons. *Journal of Applied Physics*, 122(11):114902, 2017. doi: [10.1063/1.4986409](https://doi.org/10.1063/1.4986409).
- [19] P. Murti, H. Hyodo, and T. Biwa. Suppression of liquid surface instability induced by finite-amplitude oscillation in liquid piston Stirling engine. *Journal of Applied Physics*, 127(15):154901, 2020. doi: [10.1063/5.0003921](https://doi.org/10.1063/5.0003921).
- [20] Z. Wu, G. Yu, L. Zhang, W. Dei, and E. Luo. Development of a 3 kW double-acting thermoacoustic Stirling electric generator. *Applied Energy*, 136:866–872, 2014. doi: [10.1016/j.apenergy.2014.04.105](https://doi.org/10.1016/j.apenergy.2014.04.105).
- [21] S. Rulik, W. Wróblewski, and K. Rusin. A numerical study of the relation between the acoustic generator geometry and the heat transfer conditions. *Archive of Mechanical Engineering*, 65(1):5–26, 2018. doi: [10.24425/119407](https://doi.org/10.24425/119407).
- [22] T. Bi, Z. Wu, L. Zhang, G. Yu, E. Luo, and W. Dei. Development of a 5 kW traveling-wave thermoacoustic electric generator. *Applied Energy*, 185:1355–1361, 2017. doi: [10.1016/j.apenergy.2015.12.034](https://doi.org/10.1016/j.apenergy.2015.12.034).
- [23] S. Zare, A. Tavakolpour-Saleh, and A. Omidvar. From Beale number to pole placement design of a free piston Stirling engine. *Archive of Mechanical Engineering*, 64(4):499–518, 2017. doi: [10.1515/meceng-2017-0029](https://doi.org/10.1515/meceng-2017-0029).
- [24] H. Bruus. *Theoretical Microfluidics*. Oxford University Press, Oxford, 2008.
- [25] H.-S. Yang. Numerical model for predicting the performance and transient behavior of a gamma-type free piston Stirling engine. *Applied Thermal Engineering*, 185:116375, 2021. doi: [10.1016/j.applthermaleng.2020.116375](https://doi.org/10.1016/j.applthermaleng.2020.116375).

- 
- [26] H. Joorabli, G.B. Gharehpetian, S. Ghassem-Zadeh, and V. Ghods. A new control method for distortions compensation and power control using microgrid connecting voltage source converters. *Sustainable Energy Technologies and Assessments*, 47:101373, 2021. doi: [10.1016/j.seta.2021.101373](https://doi.org/10.1016/j.seta.2021.101373).
- [27] A. Tavakolpour-Saleh and S. Zare. Justifying performance of thermo-acoustic Stirling engines based on a novel lumped mechanical model. *Energy*, 227:120466, 2021. doi: [10.1016/j.energy.2021.120466](https://doi.org/10.1016/j.energy.2021.120466).